Modelling of Spatially Offset Raman Spectroscopy effects

P. Matousek[1], M. D. Morris[2], N. Everall[3], I. P. Clark[1], M. Towrie[1], E. Draper[4], A. Goodship[4] and A. W. Parker[1]

[1]   *Central Laser Facility, CCLRC Rutherford Appleton Laboratory, Chilton, Didcot, Oxfordshire, OX11 0QX, UK*

[2]   *Department of Chemistry, University of Michigan, Ann Arbor, MI 48109, USA*

[3]   *ICI PLC, Wilton Research Centre, Wilton, Redcar, Cleveland, TS10 4RF, UK*

[4]   *Royal Veterinary College, Hawkshead Lane, North Mymms, Hatfield, Hertfordshire, AL9 7TA, UK*

Main contact email address p.matousek@rl.ac.uk

Introduction

Recently we proposed a simple method for retrieving the pure Raman spectra from subsurface layers of diffusely scattering media, Spatially Offset Raman Spectroscopy (SORS)[1]. The technique is based on the collection of a set of Raman spectra from surface regions of sample that are at set distances away from the point of illumination by the laser. The Raman spectra obtained in this way exhibit a variation in the relative intensities of the Raman spectra of the surface and sub-surface layers. The set of spectra can be subsequently processed using a multivariate data analysis method to yield estimates of the pure Raman spectra of individual sample layers. The method is parallel to several other spectroscopic approaches employed for the subsurface probing of turbid media based on NIR absorbance[2] or fluorescence spectroscopy[3,4,5]. Potential applications include biomedical subsurface interrogation of tissue such as bone disease diagnosis, dermatological studies as well as research of polymer blends, filled materials and catalysts. In this report we present the results of numerical simulations providing a comprehensive picture of basic SORS mechanism. A full account of this work is given in reference[6].

Model Description

The numerical simulations are performed using the Monte Carlo method. Both the elastically (laser) and non-elastically (Raman) scattered photons are individually followed as they propagate through the medium in a random walk-like fashion in three-dimensional space. A similar approach was adopted by Pfeifer *et al.*[3] in modelling the retrieval of fluorescence spectra of subsurface layers in a similar geometry. In our approach, a simplified assumption is made that in each step a photon propagates in a straight line over a distance t and thereafter its direction is fully randomised at the next scattering event. The propagation distance, t, over which the photon direction is randomised, can be very crudely approximated as the transport length of the scattering medium (l_t)[7,8].

The model considers the sample to be a semi-infinite turbid medium with an air-medium interface located at $z=0$, where z is a Cartesian coordinate normal to the interface plane. The top layer (thickness d) is located at depths $-d<z<0$ and the bottom layer at depth $z<-d$. The model assumes that all the probe photons are first placed in a depth equal to the transport length l_t and distributed around the origin of the co-ordinate system x,y. The beam radius of the incident light is r and the beam has uniform intensity across it, i.e. we assume it has a flat, 'top-hat' intensity profile with all the photons having equal probability of being injected into the sample at any point within its cross-section.

At each propagation step there is a given probability that the photon will be converted to a Raman photon or absorbed. When a probe photon is converted into a Raman photon the layer where this occurred is identified and recorded. A typically dominant mechanism of photon escape exists at the sample-to-air interface, as all the laser photons emerging from the sample at this interface do not return back into the sample and are effectively lost from the migration process. This effect is also accounted for in the model.

In our model, the Raman light is collected in the backscattering geometry through concentric annuli, with radii (s) equal to the SORS spatial offset as described earlier (Fig 1)[1]. This is clearly the most effective method of collecting SORS spectra. This can be approximated in practice using a collection system consisting of an array of multiple optical fibres, forming either a single annulus or a concentric set.
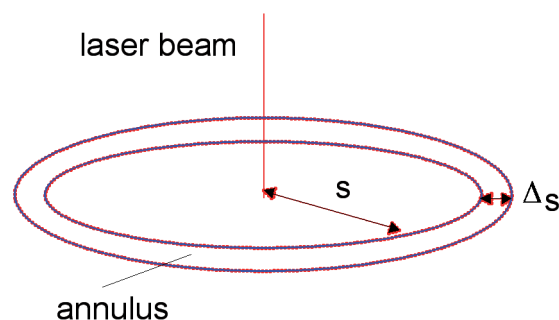

Figure 1. Definition of collection annulus for Raman scatter.

In each calculation 1000 photons were propagated simultaneously, each over an overall distance of 250 mm. The step size, t, was set at 0.2 mm unless stated otherwise (i.e. 1250 steps). This process was repeated 1000-times. The model is similar to our more comprehensive code for Raman photon migration[9] but is deliberately much simpler to enable much longer propagation distances to be investigated within time restrictions imposed by the available computing power.

Unless stated otherwise the basic conditions were as follows: the probe beam radius $r = 0$ mm, optical density accounting for the conversion of probe photons into Raman photons was 0.005 mm^{-1} chosen to exhaust the majority of probe photons over the overall propagation distance of 250 mm. The depth of the top layer was 1 mm. The thickness (Δs) of the concentric annuli through which Raman photons were counted was assumed to be 0.5 mm in each case and its inner radius was defined as the spatial offset, s, plotted in the graphs. The annuli were centred around the launch point of the probe beam into the sample.

Results and Discussion

Raman Signal Variation with SORS Spatial Offset

Figure 2a shows the dependence of Raman signal intensities from the individual layers for the annular Raman collection geometry. The initial rise of Raman intensities with spatial offset s is entirely due to the increase in the annular area ($\pi(2s\Delta s+\Delta s^2)$) outbalancing the loss of Raman signal with increasing spatial offset. Ultimately, however, the signal does start to decrease, due to a much faster fall off of Raman signal intensity in relation to the increase of the photon counting area.

As expected, the initial rise fully disappears if a point collection is adopted, figure 2b, in which photons are collected through points of negligible and constant dimensions at various spatial offsets, rather than through the annuli [1]. The signal in the point collection geometry was simulated by computing the number of Raman
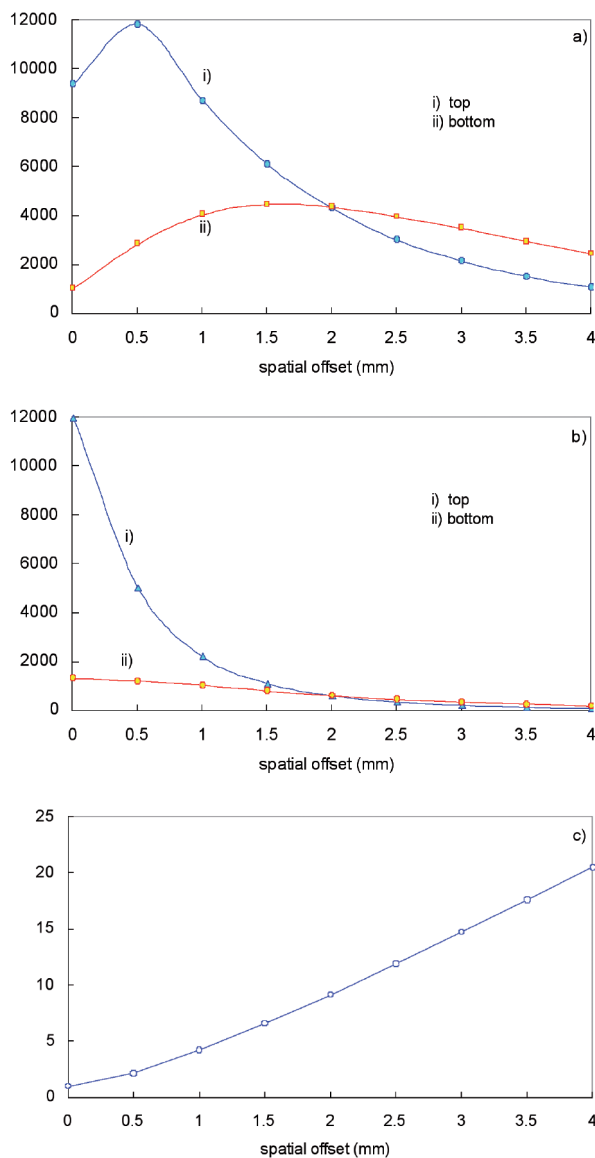

Figure 2. The dependence of Raman signal from (i) top and (ii) bottom layers on the SORS spatial offset a) for the annular Raman collection geometry, b) for the point-like Raman collection geometry. c) The variation of relative intensities of Raman spectra from the top and bottom layers expressed as the SORS ratio.

photons within each SORS annulus, normalised relative to the annulus area.

Figure 2c shows the dependence which is the most pertinent for the retrieval of Raman signals from the subsurface layers, that is, the variation of the relative Raman intensities between the bottom and top layers that contributes to the overall observed spectrum expressed in terms of the Raman signal intensity ratio of the bottom, $I_{bottom}(s)$, over the top, $I_{top}(s)$, layers for a given spatial offset, s, divided by the ratio between the same quantities with the zero spatial offset. We will refer to this parameter as the *SORS ratio*, given by:

$$SORS\ ratio(s) \quad = \quad (\frac{I_{bottom}(s)}{I_{top}(s)})/(\frac{I_{bottom}(0)}{I_{top}(0)}) \quad (1)$$

where s is the spatial offset and 0 indicates zero spatial offset.

The variation of the SORS ratio (Eq. 1) with the spatial offset is due to the (expected) faster decrease of the Raman signal from the top layer compared to that from the bottom layer, as can be seen from Figures 2a and b. For the analysed sample geometry, this results in a SORS ratio of ~10 for a spatial offset of only 2 mm (see figure 2c).

From figures 2a and b it is evident that the annular collection geometry is far superior as it yields a much smaller decrease of Raman signals as the spatial offset is increased. In fact, even with a spatial offset of 5 mm (not shown), which yields a massive 26-times variation in the SORS ratio, the intensity of the bottom layer Raman signal remains virtually unchanged compared to that at zero spatial offset and the top layer Raman signal is lowered in intensity to a still reasonable 6 % of its initial intensity at s=0. In contrast, the point-like collection geometry sees the top and bottom layer signals rapidly diminishing, and at 5 mm spatial offset they have fallen to mere 0.3% and 8% of their zero offset signals, respectively, giving much poorer S/N.

Dependence on Top Layer Thickness

Figures 3 a and 3b show how the Raman signal intensities of the top and bottom layers vary with spatial offset, s, for different thicknesses of the top layer in the point-like collection geometry. The increase of the thickness leads to only a modest improvement in the top layer Raman signal but the bottom layer signal strength dramatically decreases. Surprisingly, the SORS ratio is largely independent of the top layer thickness as is evident from figure 3c. This is a result of the fact that the ratio of the top and bottom layer signals scales in the same way with increasing top layer depth for all the spatial offsets. Consequently, and very conveniently, the ultimate usable penetration depth with the SORS methodology will only be governed by the availability of signal from the bottom layer, as the SORS ratio does not deteriorate with increasing layer thickness.

Transport Length Dependence

The dependence of Raman signal intensities of the top and bottom layers on spatial offset for different transport lengths in the point-like geometry is shown in figures 4a and 4b. The plots show the presence of a rather strong dependence on transport length, with the Raman intensity decreasing with increasing spatial offset, this decrease
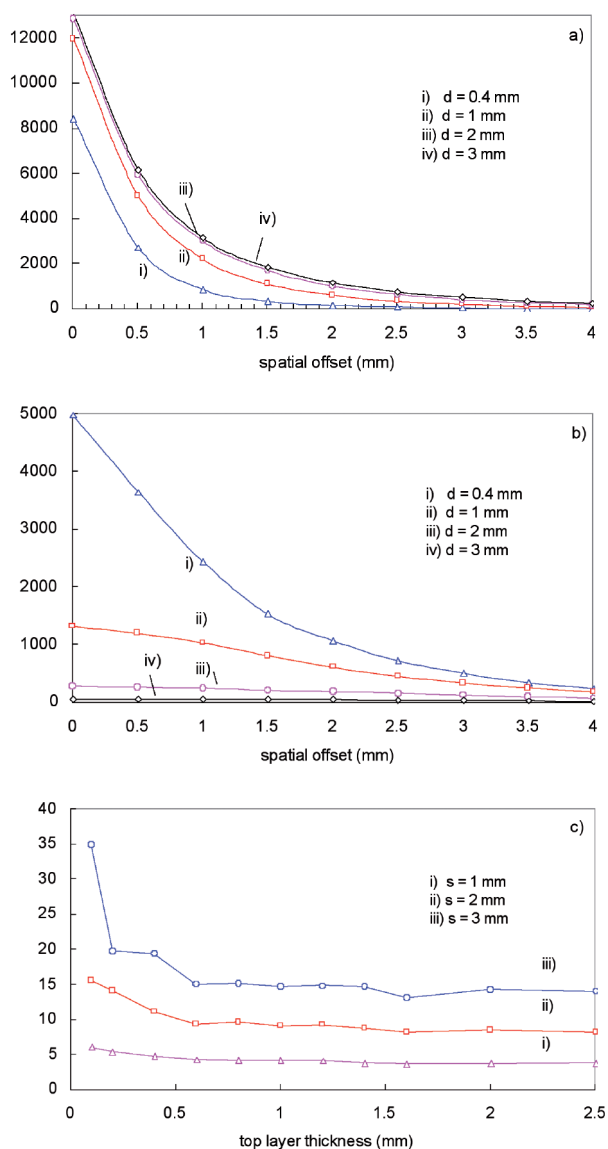
Figure 3. Variation of SORS signal with spatial offset for Raman signals originating from the a) top and b) bottom layers for different top layer thicknesses indicated in the frames. c) The dependence of the SORS ratio on the top layer thickness for three different spatial offsets indicated in the frame. The bottom layer is assumed to be semi-infinite.

Figure 4. Variation of SORS signal with spatial offset for Raman signals originating from the a) top and b) bottom layers for different transport lengths indicated in the frames. c) The dependence of the SORS ratio on the transport length for three different spatial offsets indicated in the frame.

becomes slightly shallower for longer transport lengths. Figure 4c shows that for any given spatial offset, s, the SORS ratio gradually diminishes with the increasing transport length. The relatively strong dependence of these parameters on transport length also means that the SORS technique can be utilised to measure the sample transport length if sample layer thicknesses are known. In these simulations, the transport length was assumed to be identical in both the surface and subsurface layers, which may not be the case for a real system.

Beam Radius Dependence
Predictably, the SORS ratio diminishes upon the increase of the probe beam radius and is approximately constant and equal to 1 for spatial offsets smaller than the beam radius r (see figure 5). For practical purposes, it can be stated that the beam radius should be substantially smaller than the spatial offset employed in SORS spectroscopy
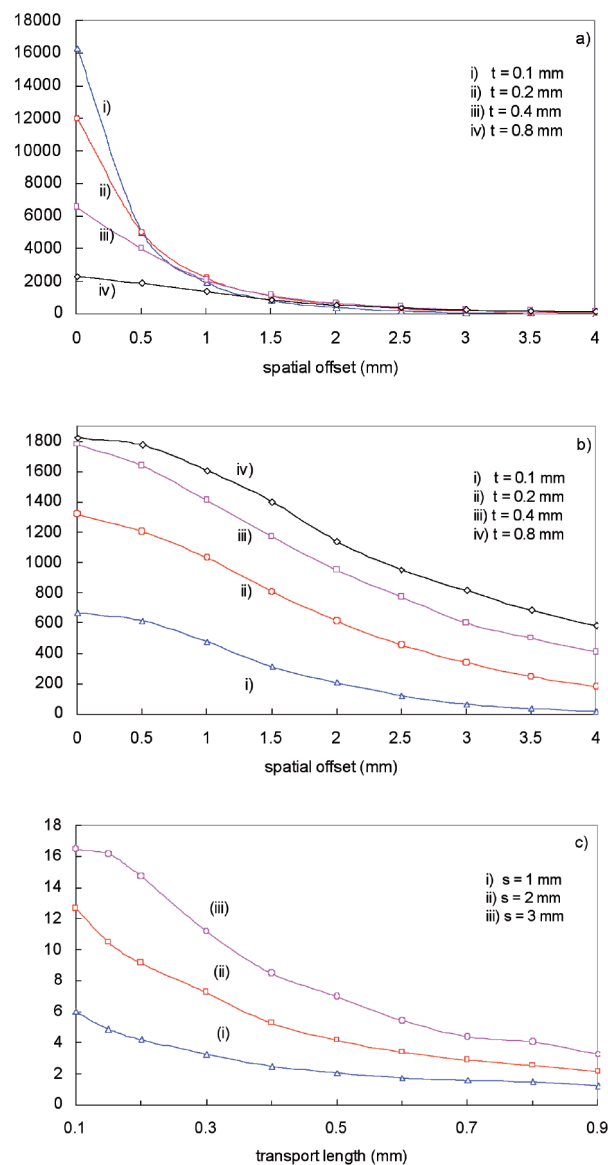
although a moderately large beam radii relative to the spatial offset would be tolerable at the expense of the diminishment of the SORS ratio.

Comparison with Experimental Data
To validate the model we compared its prediction against experimental data acquired earlier in point collection geometry[1]. Given the fact that only crude predictions were originally expected from the code, the SORS ratios, yielded by the model (calculated for 300 mm diameter probe beam) mimic reasonably well the experimental observations (see figure 6). It should be noted that no parameters have been adjusted in order to fit the experimental data, and all the input parameters in the simulations are values obtained from the experiment. Given this fact and the simplicity of the model, the good match (both qualitatively and quantitatively) is remarkable. This highlights the fact that the origin of the
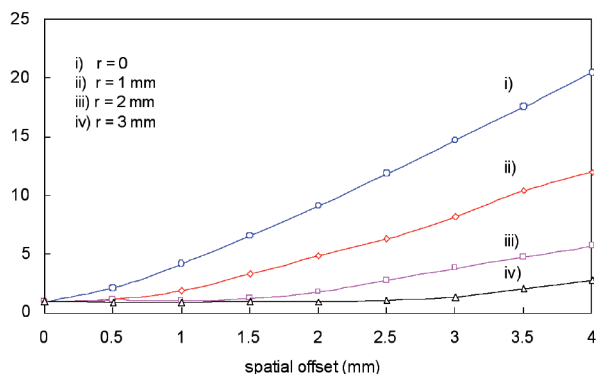
Figure 5. Variation of SORS ratio with spatial offset for four different probe beam radii indicated in the frames. The beam profile is assumed to be the top-hat.

Figure 6. Comparison of theoretical and experimental results for a two-layer system.

variation with spatial offset of the relative intensities of the Raman spectra of different layers is entirely due to randomness in the propagation of the photons within the medium and the loss of photons at the air-sample interface the key effects considered in the simulation[1]. The strong forward scattering of the actual scattering events does not influence the SORS variation with spatial offset, provided a reasonable estimate of the randomisation length t is used. An overestimation of the SORS ratio and the underestimation of Raman intensities for higher spatial offsets is ascribed to the crude nature of the simulations. The transport length of the top layer was estimated previously to be ~200 mm[1].

Conclusions

The basic numerical model depicting the evolution of Raman spectral intensities with spatial offset in Spatially Offset Raman Spectroscopy (SORS) has been described. The model reproduces very well all the key effects observed in SORS measurements, namely the dependence of Raman signal on spatial offset and the variation of relative Raman intensities between the top and subsurface-layers. A good match was also obtained between calculated relative Raman intensities and experimental data obtained using a point collection geometry. Implementing an annular geometry should greatly improve the experimental spectra that can be acquired. The model also indicates that various sample parameters such as layer depth and the transport length of the medium could also be derived from SORS observables.
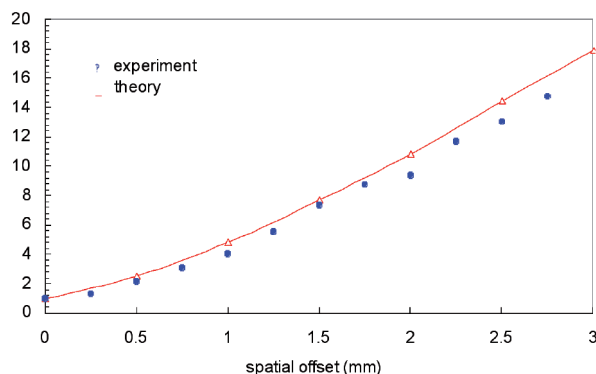
References

1. P. Matousek, I. P. Clark, E. R. C. Draper, M. D. Morris, A. E. Goodship, N. Everall, M. Towrie, W. F. Finney and A. W. Parker, *Appl. Spectrosc.* **59**, 393 (2005)
2. H. Koizumi, Y. Yamashita, A. Maki, T. Yamamoto, Y. Ito, H. Itagaki and R. Kennan, *J. Biomed. Opt.* **4**, 403 (1999)
3. T. J. Pfefer, K. T. Schomacker, M. N. Ediger and N. S. Nishioka, *Appl. Opt.* **41**, 4712 (2002).
4. N. Ghosh, S. K. Majumder, H. S. Patel and P. K. Gupta, *Opt. Lett.* **30**, 162 (2005).
5. L. Quan and N. Ramanujam, *Opt. Lett.* **27**, 104 (2002).
6. P. Matousek, M. D. Morris, N. Everall, I. P. Clark, M. Towrie, E. Draper, A. Goodship and A. W. Parker, *Appl. Spectrosc.* **59**, 1485 (2005).
7. C. J. H. Brenan and I. W. Hunter, *J. Raman Spectrosc.* **27**, 561 (1996).
8. B. B. Das, F. Liu and R. R. Alfano, *Rep. Prog. Phys.* **60**, 227 (1997).
9. N. Everall, T. Hahn, P. Matousek, A. W. Parker and M. Towrie, *Appl. Spectrosc.* **58**, 591 (2004).